JOURNAL OF MAGNETIC RESONANCE **125,** 332–339 (1997)
ARTICLE NO. MN971117

Quantification of Maximum-Entropy Spectrum Reconstructions

PETER SCHMIEDER,* ALAN S. STERN,† GERHARD WAGNER,‡ AND JEFFREY C. HOCH†,§

*Forschungsinstitute für molekulare Pharmakologie, Alfred-Kowalke-Strasse 4, D-10315 Berlin, Germany; †Rowland Institute for Science, 100 Edwin H. Land Boulevard, Cambridge, Massachusetts 02142; and ‡Department of Biological Chemistry and Molecular Pharmacology, Harvard Medical School, 240 Longwood Avenue, Boston, Massachusetts 02115

Received December 24, 1996

Maximum-entropy spectrum reconstruction derives much of its power from its nonlinearity. This nonlinearity causes difficulties in several contexts, however, including computation of multidimensional spectra and quantification of reconstructed spectra. We describe two methods for avoiding these difficulties: a "Constant-λ" algorithm for performing row-wise reconstructions, which uses a fixed weighting of the entropy and the experimental constraint in the objective function, and *in situ* error analysis, for calibrating the nonlinearity. These methods are applied to data from quantitative *J*-correlation and relaxation experiments.

INTRODUCTION

Maximum-entropy (MaxEnt) reconstruction is a powerful method for spectrum analysis that avoids some of the shortcomings of classical methods based on the discrete Fourier transform (DFT) (*1–31*). Among its properties are the ability to estimate high-resolution spectra from short data records, to deconvolve spectra without enhancing the noise, and to estimate spectra from time series that have not been sampled in a uniform fashion. An intrinsic characteristic of MaxEnt is that it is nonlinear, and the extent of the nonlinearity depends on the data and on the values of adjustable parameters used in the reconstruction. While this nonlinearity is directly responsible for some desirable properties of MaxEnt reconstruction, it also causes some problems.

The major difficulty with MaxEnt resulting from nonlinearity is that the integrated areas or volumes of peaks are not proportional to the amplitudes of the spectral components. Obviously, this complicates the use of MaxEnt reconstruction for quantitative applications, such as quantitative *J*-correlation (*32*) or relaxation-time measurements (*33, 34*). A solution to this problem would permit us to realize the benefits of nonlinear sampling (*11–14, 25, 27–29*) in these applications.

A further difficulty arises in the row- or column-wise reconstruction of multidimensional spectra. With linear methods such as the DFT, a transform can be computed by successive application of a one-dimensional DFT to the individual rows; linearity ensures that the response is proportional to the amplitude of the spectral components and that the rows can be processed independently. If MaxEnt is applied carelessly to individual rows, the extent of the nonlinearity will vary between rows, distorting peak shapes and, more importantly, rendering accurate quantification almost impossible.

Remedies exist for both of these difficulties. To ensure that the nonlinearity is uniform throughout the spectrum, one simply needs to apply MaxEnt reconstruction to the entire spectrum as a whole (holistic reconstruction), rather than row- or column-wise. The problem with this approach is that the computation of the MaxEnt reconstruction requires intermediate storage many times larger than the size of the final spectrum, rendering the demands for memory so great that supercomputer-class machines are required. Quantitative application of MaxEnt reconstruction is possible by adjusting the parameters for the reconstruction to yield nearly linear reconstructions, at the expense of some of the desirable features of MaxEnt (such as noise or artifact reduction), or by Bayesian analysis of the results to arrive at estimates of the true amplitudes of the spectral components (*20, 21*).

In this paper, we describe two simple methods for surmounting difficulties resulting from the nonlinearity inherent in MaxEnt reconstruction. The first is an algorithm which ensures that the nonlinearity of MaxEnt reconstruction is the same for all rows or columns, thereby permitting a row-wise reconstruction that is essentially equivalent to the result that would be obtained by computing the holistic reconstruction. This algorithm is well suited to workstation-class computers found in many laboratories. The second method, which we call *in situ* calibration (*31*), allows correction for the nonlinearity by adding signals of known amplitude to the time-domain data prior to reconstructing the spectrum. Using the known peaks for calibration, one can obtain reliable estimates of the amplitudes of spectral components. In addition,

§ To whom correspondence should be addressed.

1090-7807/97 $25.00

in situ error analysis facilitates estimation of the uncertainties in the results.

We will demonstrate the application of these methods to two types of NMR experiments: quantitative *J*-correlation (HNHA) (*32*) and a relaxation-time series (*33, 34*). In both cases, results obtained using linear sampling in the indirect dimension are compared with those using nonlinear sampling. We find that the quantitative *J*-correlation results are not very sensitive to the nonlinearity of MaxEnt reconstruction, in contrast to the relaxation measurements, for which some form of calibration appears to be essential.

OVERVIEW OF MAXENT RECONSTRUCTION

The details of MaxEnt reconstruction of NMR spectra have recently been described elsewhere (*30, 31*). Here we present a brief overview.

MaxEnt reconstruction of a spectrum is a problem in constrained optimization: Find the spectrum $\mathbf{f}$ which maximizes the entropy $S(\mathbf{f})$, subject to the constraint that $\mathbf{f}$ is consistent with the measured data. The consistency of the spectrum with the measured data can be quantified by defining ''mock data'' $\mathbf{m}$ obtained from $\mathbf{f}$ by inverse Fourier transformation (IDFT), and requiring that the mock data match the actual data $\mathbf{d}$ to within the expected experimental error. The match can be measured by the unweighted χ-squared statistic

$$C(\mathbf{f}) = \sum_{i=1}^{N} |m_i - d_i|^2 = \sum_{i=1}^{N} |\mathrm{IDFT}(\mathbf{f})_i - d_i|^2, \quad [1]$$

where the data $\mathbf{d}$ has N elements d_i (the mock data may have more than N elements). The spectrum $\mathbf{f}$ is considered consistent with $\mathbf{d}$ if $C(\mathbf{f}) \leqslant C_0$, where C_0 is determined by the experimental error. Typically, C_0 is comparable to the number of points in the data set times the square of the expected error for each point. For convenience, we will generally refer to *aim* instead of C_0; *aim* is defined as $\sqrt{C_0/2N}$ and is comparable to the expected error in each component (real and imaginary) of each point in the data set.

The entropy has the form

$$S(\mathbf{f}) = -\sum_{i=1}^{M} R(f_i), \quad [2]$$

where R is a function resembling $R(z) = (|z|/def)\log(|z|/def)$, M is the number of points in the spectrum, and *def* is a scale factor. The actual functional form of R is more complicated but irrelevant to the present discussion (*31*). The constrained-optimization problem is solved by maximizing the objective function

$$Q(\mathbf{f}) = S(\mathbf{f}) - \lambda C(\mathbf{f}), \quad [3]$$

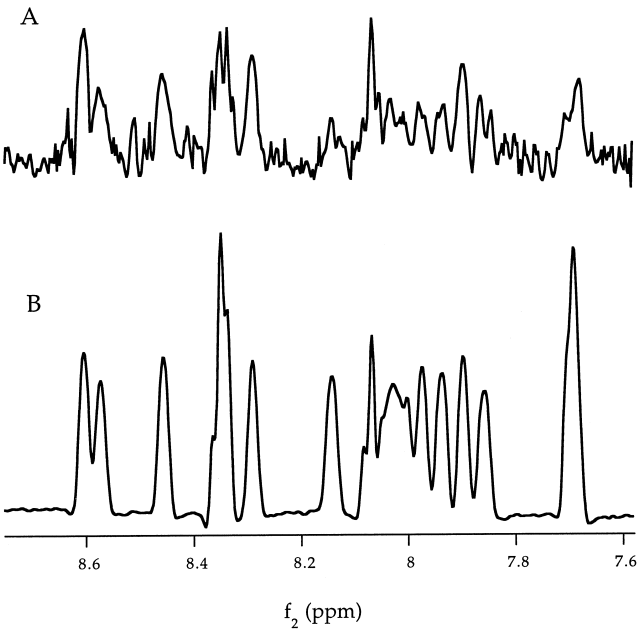

FIG. 1. (A) The value of λ as a function of f_2 chemical shift obtained from a Constant-*aim* (see text) MaxEnt reconstruction in f_1 of NOESY data for a small protein. (B) $t_1 = 0$ cross section from the $t_1 - f_2$ interferogram used as input for the reconstruction. The value of λ is clearly correlated with the signal intensity.

where λ is a Lagrange multiplier that determines the relative weight of the entropy and the constraint that $C(\mathbf{f}) \leqslant C_0$. (Because the entropy functional is convex, there is a unique global solution, and it satisfies $C(\mathbf{f}) = C_0$.) The value of λ is chosen so that at the maximum of Q, we have $C(\mathbf{f}) = C_0$. The parameters of the reconstruction are the constraint value C_0 (or equivalently, *aim*), the scale factor *def*, and the size of the spectrum M.

The constrained-optimization problem cannot be solved analytically. Several numerical algorithms have been published (*4, 17, 18, 31*). They all work by iteratively improving a trial guess of the spectrum and simultaneously adjusting λ so as to arrive at a final solution satisfying the criteria above.

THE CONSTANT-λ ALGORITHM

An interesting feature of the method of Lagrange multipliers is that it provides a family of potential solutions to the constrained-optimization problem. Each value for the Lagrange multiplier λ will give rise to a spectrum $\mathbf{f}_\lambda$. This $\mathbf{f}_\lambda$ maximizes Q (and hence S) among all spectra $\mathbf{g}$ having $C(\mathbf{g}) = C(\mathbf{f}_\lambda)$. The correct value of λ is the one for which $C(\mathbf{f}_\lambda)$ is equal to the desired value C_0. Although it is not explicitly indicated by our notation, Eq. [1] shows that the value of $C(\mathbf{f})$ depends on the experimental data $\mathbf{d}$ as well as on $\mathbf{f}$. Consequently, the desired value for λ will depend on the data, as can be seen in Fig. 1.

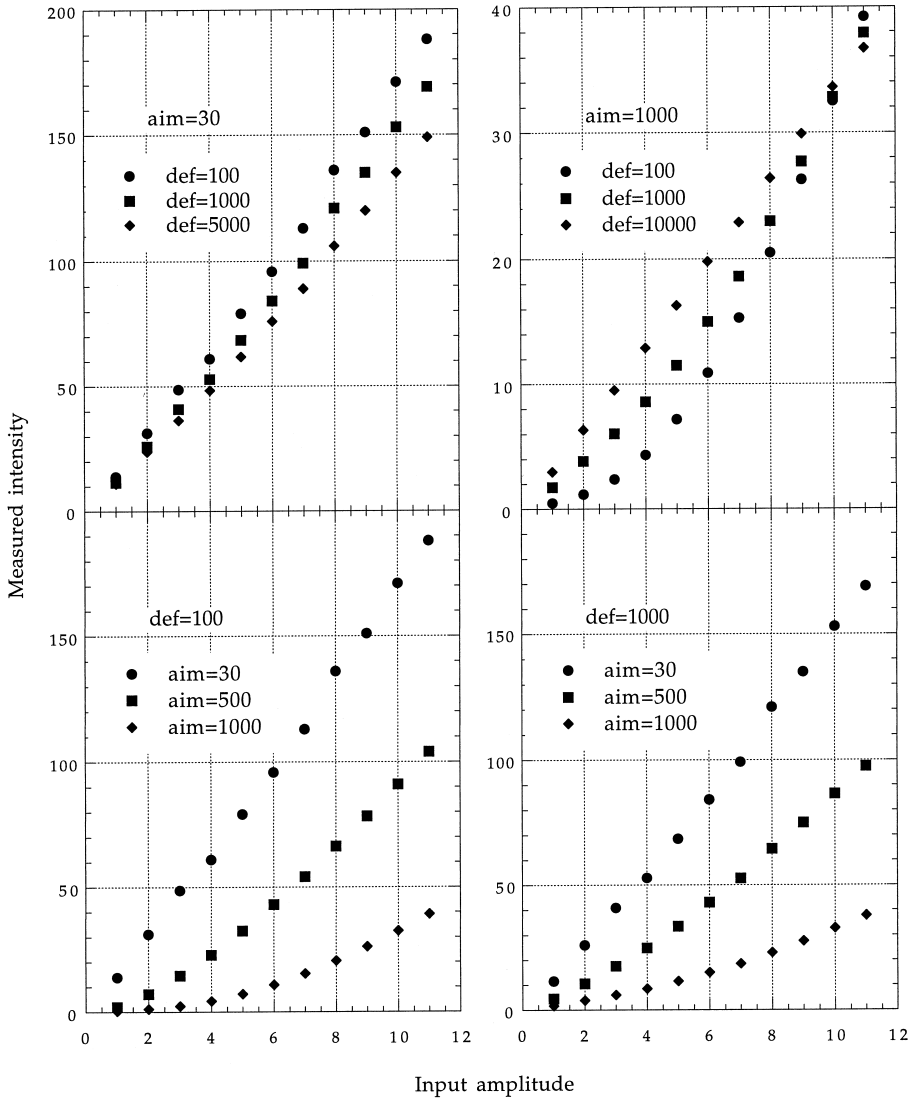

FIG. 2. The *in situ* calibration curves obtained for a synthetic data set, showing the dependence of the nonlinearity of MaxEnt reconstruction on the parameters *def* and *aim*. The two-dimensional data set consisted of 512 complex points in t_2 and 256 complex points in t_1, with a spectral width of 2000 Hz in both dimensions. The synthetic signals comprised 11 exponentially decaying sinusoids having linewidths of 10 Hz in both dimensions, with evenly spaced amplitudes. Gaussian random noise (RMS = 30) was added to the signals. Cosine-squared-bell apodization was applied in t_2 prior to Fourier transformation, and holistic MaxEnt reconstruction was used in f_1, with a spectrum length of 512 points. Peak intensities were determined by volume integration.

Now consider a multidimensional data set which has been transformed to the frequency domain in every dimension except one, which we will call the active dimension. To perform a Fourier transform along the active dimension, one can extract individual vectors (i.e., rows) parallel to the active axis and process each independently as if it were a one-dimensional data set. Row-wise MaxEnt reconstruction works in the same way: For each vector, the sums in Eqs. [1] and [2] range only over points in the individual vector, rather than over the entire spectrum (as they would for holistic reconstruction). There is no meaningful difference between row-wise and holistic application of the Fourier transform; for MaxEnt reconstruction however, the two approaches will generally yield different results.

A detailed comparison of the computations involved illustrates the relation between the two approaches. Let $f_{i_1,\ldots,i_n}$ be a point from the vector under consideration. From the form of Eq. [2], it is clear that

$$\nabla S^{\mathrm{R}}(f)_{i_1,\ldots,i_n} = \nabla S^{\mathrm{H}}(f)_{i_1,\ldots,i_n}, \qquad [4]$$

where ∇S^{R} is the gradient of the entropy for the row-wise reconstruction and ∇S^{H} is the gradient for the holistic recon-

struction. Computation of the gradient of the constraint is more complicated, since it requires transforming the trial spectrum to the time domain in order to evaluate Eq. [1]. Nevertheless, since the transformation is along the active dimension, the value of the gradient at any particular point depends only on points in the same vector. Consequently,

$$\nabla C^{\mathrm{R}}(f)_{i_1,\ldots,i_n} = \nabla C^{\mathrm{H}}(f)_{i_1,\ldots,i_n}. \qquad [5]$$

This means that for any value of λ, the same spectrum **f** will maximize $Q(\mathbf{f})$ for both the row-wise and holistic reconstructions. Thus, the only difference is that for row-wise reconstruction, different values of λ will apply to different rows (since λ depends on the data), whereas for holistic reconstruction, a single value of λ applies to the entire spectrum. Consequently, in a row-wise reconstruction, the nonlinearity varies from row to row, since the relative weight applied to the entropy and the constraint differs from row to row. The manifestations are often subtle, but they can be important when quantitative analysis is performed.

This analysis indicates how to obtain the benefits of holistic reconstruction—namely, a uniform nonlinearity—at the low expense of a row-wise computation. Rather than adjusting λ to obtain $C(\mathbf{f}) = C_0$, one should use a single fixed value of λ for all rows of the data set. This is the Constant-λ algorithm. Making this change simplifies the computation, as it removes the need to search over λ; however, it introduces the problem of finding the appropriate value for λ. A reasonable approach is to select a representative row from the data, compute a normal MaxEnt reconstruction of that row, and use the resulting value of λ. The final spectrum will not satisfy $C(\mathbf{f}) = C_0$ exactly, but it should be close if the representative row is sufficiently typical.

An additional advantage of the Constant-λ algorithm arises in the analysis of multiple spectra, for example, a relaxation series. Holistic reconstruction of the series would use different values of λ for the different spectra, thereby introducing unwanted intensity variation. With the Constant-λ algorithm, on the other hand, a single value of λ can be used for all the spectra in the series.

The Constant-λ algorithm is a row-wise procedure. We will use the term ''Constant-*aim*'' to refer to row-wise reconstructions as originally described—i.e., in which λ is allowed to vary between rows so as to achieve $C(\mathbf{f}) = C_0$ for each row.

IN SITU CALIBRATION

To take proper account of the nonlinearities introduced by MaxEnt reconstruction, it is necessary to calibrate the intensities of the spectral peaks. With *in situ* error analysis (*31*), this calibration is accomplished by adding synthetic signals of known amplitude to the raw data, and comparing the intensities of the resulting peaks with those of the true signal components. The synthetic signals take the form of exponentially decaying sinusoids, with phases and decay rates (or linewidths) chosen to be similar to those of the true signals, and frequencies chosen to avoid overlap. The amplitudes are chosen to span the range of signal peak intensities.

TABLE 1
Values of λ Resulting from Holistic Reconstruction of a Synthetic Data Set, Corresponding to the Data in Fig. 2

aim	*def*	λ
30	100	2.3300
30	1000	7.2967
30	5000	14.5945
1000	100	0.0196
1000	1000	0.0908
1000	10000	0.1784
30	100	2.3300
500	100	0.0674
1000	100	0.0196
30	1000	7.2967
500	1000	0.3069
1000	1000	0.0908

Note. For fixed *def*, λ varies inversely with *aim.*

Plotting the measured intensities of the synthetic peaks against their known amplitudes results in a calibration curve, which can be used to determine the relative intensities of the signal peaks. Since the synthetic components undergo the same processing as the signal components, they should experience the same distortions. Consequently, use of the calibration curve will provide a more accurate measure of intensities than direct use of volume or area measurements. The curve can be obtained simply by piecewise linear (or higher-order) interpolation between the measured intensities of the synthetic peaks. The accuracy of the calibration curve will depend to some extent on the number of synthetic peaks, the nature of the nonlinearity, and the form of the interpolation. The correction cannot be perfect, because the nonlinearity of MaxEnt reconstruction means that the intensity of a reconstructed peak will partly depend on factors other than the underlying signal amplitude (such as the linewidth or the density of neighboring peaks). No simple calibration curve can correct for these effects; fortunately, the residual errors appear to be acceptably small.

The *in situ* approach can be used to explore the dependence of the MaxEnt nonlinearity on the parameters *def* and *aim.* A synthetic data set was subjected to holistic MaxEnt reconstruction, with varying values of the parameters. Figure 2 shows the calibration curves, and Table 1 shows the corre-

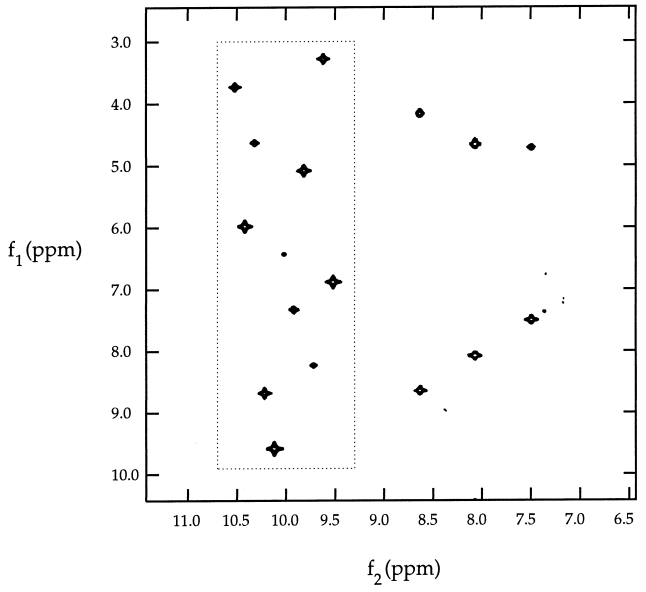

FIG. 3. A Constant-λ MaxEnt reconstruction from HNHA data recorded for a 30 m*M* sample of a cyclic hexapeptide labeled as described in the text. Data were recorded on a Bruker AMX 500 at 298 K. Sixteen transients and 1024 complex points were collected in the acquisition dimension; nonlinear sampling of 64 complex points out of a linear schedule of 256 points required 50 min. of data-acquisition time. The spectral widths were 10000 Hz in t_2 and 8000 Hz in t_1. Eleven synthetic signals, with linewidths of 10 Hz in each dimension, were added to the raw data (indicated by the dotted line). Processing in f_2 used cosine-squared-bell apodization and Fourier transformation; processing in f_1 used MaxEnt reconstruction as described in the legend to Fig. 4.

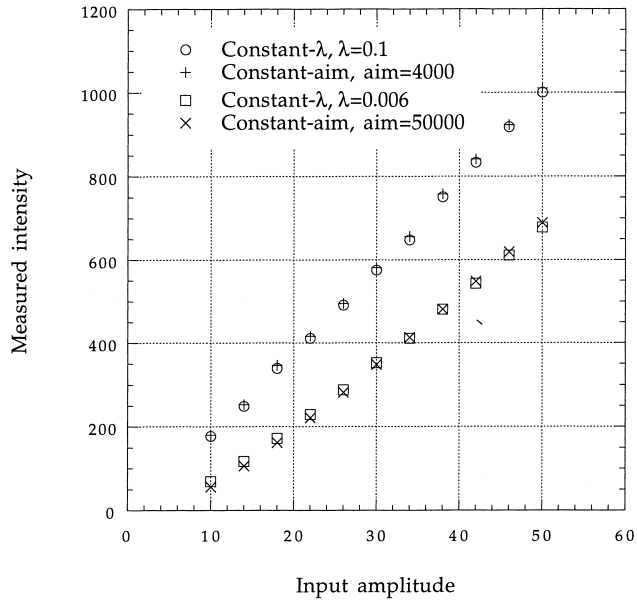

FIG. 4. Calibration data for four MaxEnt reconstructions of the spectrum shown in Fig. 3. The reconstruction shown in Fig. 3 corresponds to λ = 0.1. *Def* was set to 100 for all four reconstructions. For comparison with the indicated values of *aim*, measurement of the noise in an empty row of the data yielded an RMS value of 3900. Note that data for high values of *aim* do not lie on a line passing through the origin, indicating the greater nonlinearity of MaxEnt reconstruction in this regime.

sponding values of λ. The results demonstrate that when *aim* is close to the noise level, λ will be higher and the calibration curves more linear. A rather high value for *aim* will give the reconstruction more freedom to maximize the entropy; λ will be smaller and the reconstruction more nonlinear. High values of *def* yield more linear reconstructions than do small values, but *aim* has a greater influence on the nonlinearity. Only if *aim* is rather high can the value of *def* significantly influence the reconstruction.

RESULTS AND DISCUSSION

Quantitative J Correlation

Two-dimensional (^{1}H, ^{1}H) HNHA experiments (*32*) were performed, with and without nonlinear sampling, on the cy-

TABLE 2

$^3J_{N\alpha}$ Coupling Constants for the Cyclic Hexapeptide Whose Spectrum Is Shown in Fig. 3, Computed with and without *in Situ* Calibration of the Peak Intensities

			MaxEnt							
			Uncalibrated				Calibrated			
			Constant-λ		Constant-*aim*		Constant-λ		Constant-*aim*	
Residue	1D	2D DFT	Tight	Loose	Tight	Loose	Tight	Loose	Tight	Loose
Phe 2	8.6	8.4	8.2	7.9	8.2	8.1	8.3	8.3	8.3	8.5
Phe 3	9.6	9.4	9.2	9.1	9.2	9.2	9.3	9.2	9.3	9.3
Phe 6	6.6	6.4	6.1	5.3	6.1	5.6	6.3	6.4	6.4	6.8

Note. The column labels ''Tight'' and ''Loose'' indicate the degree to which the reconstruction was constrained to match the data; loose implies large *aim* or small λ. The calibration curves for these reconstructions are shown in Fig. 4.

clic hexapeptide cyclo-(−D−Pro−Phe−Phe−Lys(Z)−Trp−Phe−) labeled with ^{15}N in the three phenylalanine positions. The linearly sampled data set was processed by Fourier transformation, and peak intensities were determined by integrating the volumes. For a molecule of this size, quantitative J correlation yields coupling constants that are about 2−3% smaller than those obtained by measuring splittings in a one-dimensional spectrum (*32*). The nonlinearly sampled data set was processed using MaxEnt reconstruction. Constant-*aim* processing was performed using high and low values of *aim*, and Constant-λ processing was performed with low and high values of λ (corresponding roughly to the high and low *aim* reconstructions, respectively). The high-λ reconstruction is shown in Fig. 3.

The measured intensity of the injected peaks is shown in Fig. 4, demonstrating the differences caused by the choice of the parameters and the algorithm. For this data set, the differences due to the choice of parameters is substantial, but the Constant-λ and Constant-*aim* reconstructions yield very similar results. The calculated coupling constants (derived from the ratio of the cross peak and the diagonal peak intensities) are compared in Table 2. For the tightly constrained reconstructions (low *aim* or high λ), evaluation without calibration yields coupling constants that are too small; the error turns out to be relatively minor. As can be expected, the largest relative error occurs for the smallest coupling constant (Phe-6), which results from the smallest cross peak. (The effect of nonlinearity on peak ratios is more pronounced the further the ratio is from one.) The *in situ* calibration works equally well in both cases, resulting in coupling constants close to those obtained from the DFT spectrum. The more biased results that are obtained when *aim* is large can be understood on the basis of Fig. 4, which shows that the nonlinearity of MaxEnt reconstruction is more pronounced for large values of *aim*. Both loosely constrained reconstructions (high *aim* or low λ) yield coupling constants that are too small, and again the coupling constant of Phe-6 has the largest error. The coupling constant of Phe-3 (the largest coupling constant) is hardly affected. *In situ* calibration of the Constant-λ reconstruction yields acceptable coupling constants, but calibration of the Constant-*aim* reconstruction yields coupling constants that are too large. We attribute this to the fact that the nonlinearity is different in the rows that contain signal from the rows that contain the synthetic peaks. Thus, the correction that is appropriate for the synthetic peaks is not necessarily appropriate for the real intensities. This problem does not arise with Constant-λ reconstruction, since there the nonlinearity is the same throughout the spectrum.

Relaxation-Time Series

An ^{15}N relaxation-time series was recorded to determine the T_1 relaxation times of Villin 14T (*35, 36*). Two series were recorded, one using linear and one using nonlinear sampling; 12 data sets were recorded for each series. The linearly sampled data were processed by Fourier transformation, and the relaxation times were determined by fitting an exponential decay to the measured intensities. The nonlinearly sampled data were processed by MaxEnt reconstruction.

Three different types of reconstructions were performed:

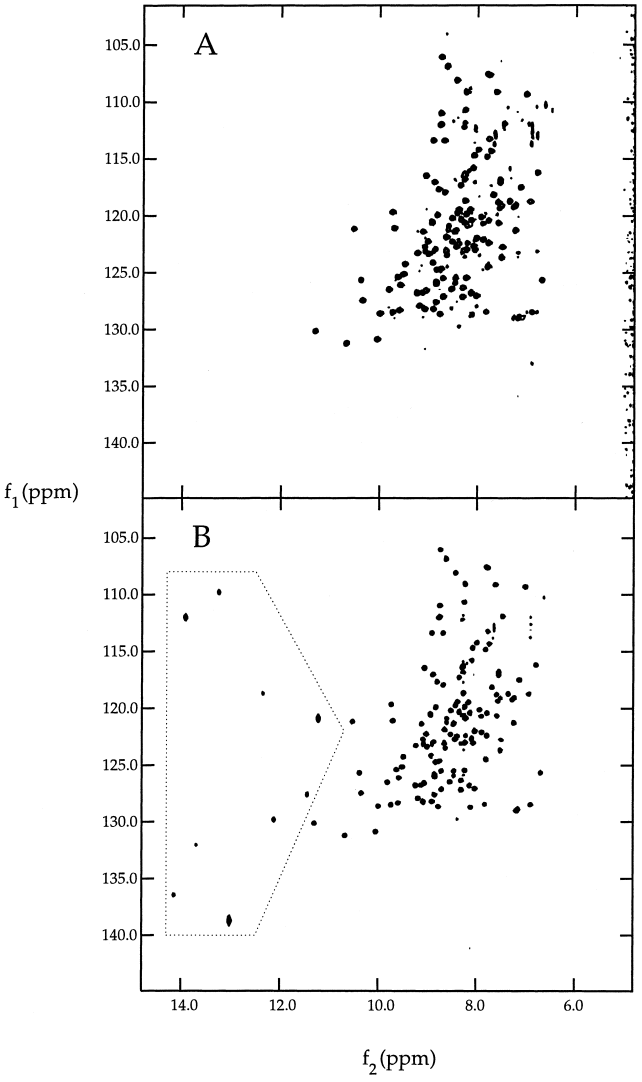

FIG. 5. 500 MHz T_1 relaxation data obtained on a Varian Unity 500 for a 1.5 m*M* solution of Villin 14T in 90% H_2O/10% D_2O. In both spectra, 1024 points were collected in the t_2 dimension and processed by 60°-shifted sine-squared-bell apodization and Fourier transformation. (A) A total of 256 linearly sampled data points in t_1 (eight transients each) processed by DFT. (B) A total of 64 nonlinearly sampled points in t_1 (16 transients each) processed by MaxEnt reconstruction. Prior to data processing, synthetic signals used to calibrate the spectrum were added to the time-domain data; they are in the region indicated by the dotted line. Note that the data for (B) required half as much time to collect as the data for (A).

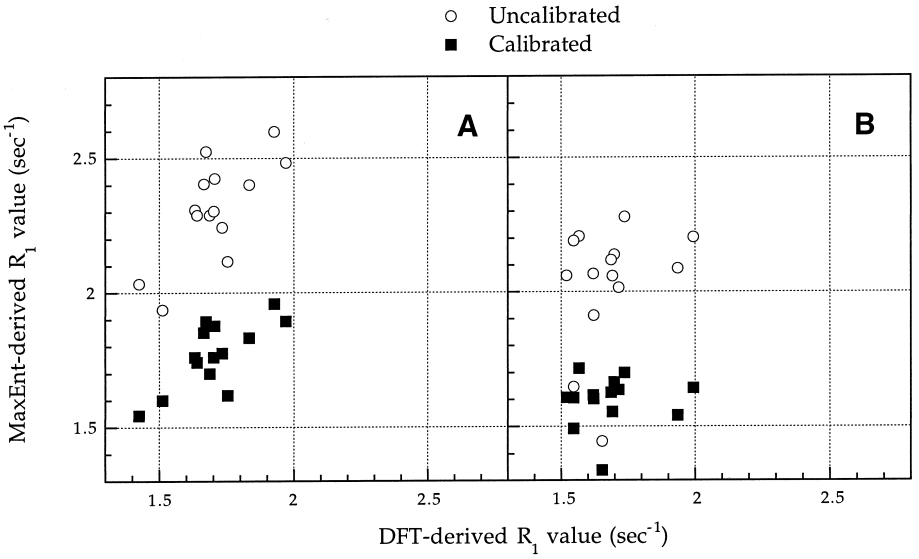

FIG. 6. Comparison of relaxation rates determined from DFT spectra and MaxEnt spectra (one of which is shown in Fig. 5). Values obtained with and without calibration of the MaxEnt spectra are shown. (A) A selection of values for cross peaks in a relatively uncrowded region of the spectrum (near 10 ppm in f_2). (B) A selection of values for cross peaks in a relatively crowded region of the spectrum (between 8 and 9 ppm in f_2). Variation in the results reflect both errors in calibration of the MaxEnt spectra and errors in quantifying peak volumes (which are more pronounced for crowded peaks).

Constant-*aim*, holistic, and Constant-λ. Calibration curves were determined independently for each spectrum of the series. Two sets of cross peaks were subjected to analysis, one consisting of peaks in an uncrowded region of the spectrum, and the other of peaks in a crowded region. One of the Constant-λ reconstructions is shown in Fig. 5, and the computed relaxation times are displayed in Fig. 6.

The results indicate that use of uncalibrated MaxEnt data for obtaining relaxation rates is ill-advised, as the rates are greatly overestimated. [This is because MaxEnt tends to shrink small values more than large ones, thereby increasing the apparent decay rate (*19*)]. Calibration yields values comparable to those obtained by conventional Fourier processing. The RMS difference in the relaxation rates computed from the DFT and calibrated Constant-λ data is 7% for the uncrowded region and 10% for the crowded region. The corresponding differences for the uncalibrated data are 37 and 26%, respectively. Errors for holistic and Constant-*aim* reconstructions are larger (data not shown). Normally, holistic reconstruction would be expected to give the same result as Constant-λ reconstruction, but this no longer holds true when comparing a series of spectra—holistic reconstruction can only guarantee that a single value of λ is used within each spectrum, not across different spectra. In this setting, Constant-λ reconstruction is therefore preferable to holistic reconstruction.

CONCLUSION

In situ calibration of MaxEnt reconstructions is able to produce reliable intensity estimates, despite the nonlinearity inherent in MaxEnt. The accuracy of the results depends on both the choice of parameters and the reconstruction algorithm. Low values of *aim* (close to the intrinsic noise level) lead to very modest nonlinearities, which may remove the need for *in situ* calibration altogether. With larger nonlinearities, intensity calibration is necessary. In these situations the Constant-*aim* algorithm yields poor results, because it leads to unpredictable variations in the nonlinearity, rendering accurate calibration impossible. Constant-λ and holistic reconstruction yield spectra that are more amenable to calibration. However, the Constant-λ algorithm has significantly lower computational demands, and is easier to implement on laboratory workstations. In addition, Constant-λ reconstruction is the only appropriate method for applications in which series of spectra are to be compared. As shown by our results, Constant-λ reconstruction in concert with *in situ* calibration permits MaxEnt to be used in contexts calling for quantification of peak intensities. Among other benefits, this opens the door to the use of nonlinear sampling to increase sensitivity, enhance resolution, or reduce data collection time.

ACKNOWLEDGMENTS

The authors thank Professor Dr. Horst Kessler and Dr. Michael Kurz for the samples of the cyclic hexapeptide and Dr. Michelle Markus for the sample of Villin 14T. P.S. thanks the Deutsche Forschungsgemeinschaft and the Fonds der Chemischen Industrie for fellowships. This work was supported by the Rowland Institute for Science, the W. M. Keck Foundation, the National Institutes of Health (Grant GM 47467), the National Science

Foundation (Grant MCB 9316938), and the Forschungsinstitut für Molekulare Pharmakologie. We are grateful to the Center for Computational Science at Boston University for providing time on a Thinking Machines CM-5 computer.

REFERENCES

1. S. Sibisi, *Nature* **301,** 134–136 (1983).
2. J. Skilling, *Nature* **309,** 748–749 (1984).
3. S. Sibisi, J. Skilling, R. G. Brereton, E. D. Laue, and J. Staunton, *Nature* **311,** 446–447 (1984).
4. J. Skilling and R. K. Bryan, *Mon. Not. R. Astron. Soc.* **211,** 111–124 (1984).
5. E. D. Laue, J. Skilling, and J. Staunton, *J. Magn. Reson.* **63,** 418–424 (1985).
6. P. J. Hore, *J. Magn. Reson.* **62,** 561–567 (1985).
7. J. C. Hoch, A. S. Stern, D. L. Donoho, and I. M. Johnstone, *J. Magn. Reson.* **64,** 436–440 (1985).
8. J. F. Martin, *J. Magn. Reson.* **65,** 291–297 (1985).
9. E. D. Laue, M. R. Mayger, J. Skilling, and J. Staunton, *J. Magn. Reson.* **68,** 14–29 (1985).
10. K. M. Wright and P. S. Belton, *Mol. Phys.* **58,** 485–495 (1986).
11. J. C. J. Barna, E. D. Laue, M. R. Mayger, J. Skilling, and S. J. P. Worrall, *Biochem. Soc. Trans.* **14,** 1262–1263 (1986).
12. J. C. J. Barna, E. D. Laue, M. R. Mayger, J. Skilling, and S. J. P. Worrall, *J. Magn. Reson.* **73,** 69–77 (1987).
13. J. C. J. Barna, E. D. Laue, M. R. Mayger, J. Skilling, and S. J. P. Worrall, *J. Magn. Reson.* **75,** 384–389 (1987).
14. J. C. J. Barna, E. D. Laue, *Lab. Pract.* **36,** 102–109 (1987).
15. D. S. Stephenson, *Prog. NMR Spectrosc.* **14,** 515–626 (1988).
16. J. C. Hoch, *Methods Enzymol.* **176,** 216–241 (1989).
17. G. J. Daniell, P. J. Hore, *J. Magn. Reson.* **84,** 515–536 (1989).
18. M. A. Delsuc, *in* ''Maximum Entropy and Bayesian Methods'' 1990 Workshop, (J. Skilling, Ed.), pp. 285–290, Kluwer Academic, Dordrecht, The Netherlands, 1991.
19. D. L. Donoho, I. M. Johnstone, A. S. Stern, and J. C. Hoch, *Proc. Natl. Acad. Sci. USA* **87,** 5066–5068 (1990).
20. J. Skilling, *in* ''Maximum Entropy and Bayesian Methods'' 1989 Workshop, (P. F. Fougère, Ed.), pp. 341–350, Kluwer Academic, Dordrecht, The Netherlands, 1990.
21. S. Sibisi, *in* ''Maximum Entropy and Bayesian Methods'' 1989 Workshop, (P. F. Fougère, Ed.), pp. 351–358, Kluwer Academic, Dordrecht, The Netherlands, 1990.
22. J. A. Jones and P. J. Hore, *J. Magn. Reson.* **92,** 276–292 (1991).
23. J. A. Jones and P. J. Hore, *J. Magn. Reson.* **92,** 363–376 (1991).
24. M. A. Delsuc, M. Robin, C. Van Heijenoort, C. B. Reisdorf, and E. Guittet, *NATO ASI Ser. Ser. A* **225,** 163–174 (1991).
25. M. Robin, M.-A. Delsuc, E. Guittet, and J.-Y. Lallemand, *J. Magn. Reson.* **92,** 645–650 (1991).
26. P. Hodgkinson, H. R. Mott, P. C. Driscoll, J. A. Jones, and P. J. Hore, *J. Magn. Reson. B* **101,** 218–222 (1993).
27. P. Schmieder, A. S. Stern, G. Wagner, and J. C. Hoch, *J. Biol. NMR* **3,** 569–576 (1993).
28. P. Schmieder, A. S. Stern, G. Wagner, and J. C. Hoch, *J. Biol. NMR* **4,** 483–490 (1994).
29. P. Hodgkinson, K. J. Holmes, and P. J. Hore, *J. Magn. Reson. A* **120,** 18–30 (1996).
30. J. C. Hoch and A. S. Stern, *in* ''Encyclopedia of NMR'' (D. M. Grant and R. K. Harris, Eds.), Vol. 5, pp. 2980–2988, Wiley, Chichester, England, 1996.
31. J. C. Hoch and A. S. Stern, ''NMR Data Processing,'' Wiley–Liss, New York, 1996.
32. G. W. Vuister and A. Bax, *J. Am. Chem. Soc.* **115,** 7772–7777 (1993).
33. N. R. Nirmala and G. Wagner, *J. Am. Chem. Soc.* **110,** 7557–7559 (1988).
34. L. E. Kay, D. A. Torchia, and A. Bax, *Biochemistry* **28,** 8972–8979 (1989).
35. M. A. Markus, T. Nakayama, P. Matsudaira, and G. Wagner, *J. Biol. NMR* **4,** 553–574 (1994).
36. M. A. Markus, T. Nakayama, P. Matsudaira, and G. Wagner, *Protein Sci.* **3,** 70–81 (1994).